Journal of Power Sources 198 (2012) 389–392

Contents lists available at SciVerse ScienceDirect

Journal of Power Sources

journal homepage: www.elsevier.com/locate/jpowsour

Short communication

Novel synthesis and electrochemical properties of perovskite-type $NaFeF_3$ for a sodium-ion battery

Ayuko Kitajou[a], Hideyuki Komatsu[b], Kuniko Chihara[c], Irina D. Gocheva[c], Shigeto Okada[c,*], Jun-ichi Yamaki[b,c]

[a] Research and Education Center of Carbon Resources, Kyushu University, 6-1 Kasuga-koen, Kasuga 816-8580, Japan
[b] Graduate School of Integrated Frontier Sciences, Kyushu University, 6-1 Kasuga-koen, Kasuga 816-8580, Japan
[c] Institute for Materials Chemistry and Engineering, Kyushu University, 6-1 Kasuga-koen, Kasuga 816-8580, Japan

ARTICLE INFO

Article history:
Received 6 July 2011
Received in revised form
20 September 2011
Accepted 21 September 2011
Available online 29 September 2011

Keywords:
Sodium-ion battery
Transition-metal fluoride
Roll-quench method

ABSTRACT

Highly crystallized perovskite-type $NaFeF_3$ has been investigated as the cathode for sodium-ion batteries through the roll-quench method. In the charge–discharge measurement, the first discharge capacity was 197 mAh g^{-1} at a rate of 0.076 mA cm^{-2} between 1.5 V and 4.5 V. Reversible Fe^{2+}/Fe^{3+} redox reaction on cycle was confirmed by XPS. The ex situ XRD measurements for charged or discharged $NaFeF_3$ pellets revealed the reversible vibration on cycle, due to the structure strength and flexibility of the corner-sharing matrix. The peak intensities of (1 1 2) and (0 0 4) were changed with accompanying insertion/extraction of sodium, suggesting the extracted sodium has returned to the original *4c* site on discharge.

1. Introduction

The demands for Li-ion batteries have been increasing in recent years due to their wide application to electric power storage for electric vehicles and small electric devices. The commercially available Li-ion batteries generally consist of lithium 3d-transition metal oxides such as $LiCoO_2$, $LiMn_2O_4$, and $LiFePO_4$ for a cathode. $LiCoO_2$ works at 3.9 V and shows an acceptably large capacity of 140 mAh g^{-1}. However, lithium and cobalt are relatively costly, and the resources of lithium and cobalt are insufficient at this point. Alternative resources should therefore be found to satisfy the expected increasing demands in the near future. A Na-ion battery, where lithium as the current carrier is substituted with sodium, is expected to provide good economical efficiency due to its high level of availability. However, the standard electrode potential of sodium (−2.71 V vs. SHE) is lower than that of lithium (−3.05 V vs. SHE); furthermore, the sodium metal is air-sensitive and the ionic volume is almost 2 times larger than that of Li-ion. Therefore, the reported cathodes against the sodium metal have been limited to narrow material groups such as two-dimensional layered compounds with a van der Waals gap, e.g. TiS_2 [1] and three-dimensional compounds with a corner-sharing matrix, e.g. FeS_2 [2]. Recently, 3d-transition-metal binary compounds, MF_3 (M = Fe [3–5], Ti [4,5], V [5], Mn [5], Co [5], and Bi [6]) have been extensively investigated as potential electrode materials. The idea to exploit fluorides as batteries arises from the intrinsic stability of fluorinated materials and their ability to generate high levels of electrochemical energy. Both of these attributes come as a direct result of the large electro-negativity and small electrochemical equivalent of fluorine. In particular, FeF_3 electrodes showed a high discharge capacity of about 200 mAh g^{-1} at approximately 3.3 V vs. lithium metal with a mixture of ethylene carbonate (EC) and dimethyl carbonate (DMC) dissolving with 1 mol dm^{-3} $LiPF_6$, which corresponds to 99% of the theoretical specific capacity (238 mAh g^{-1}) based on the FeF_3 content. Our group has previously reported that FeF_3 electrodes show a discharge capacity of 100 mAh g^{-1} vs. sodium metal in propylene carbonate (PC) dissolved with 1 mol dm^{-3} $NaClO_4$ [5]. However, FeF_3 cannot be used as cathodes against pristine carbonaceous materials, which are practically used in the Li-ion battery as negative electrodes, because of the lack of lithium or sodium for the current carrier. Recently, Li-containing negative electrode materials have been widely studied, but it may take time to establish them as commercial materials. Therefore a lithium/sodium containing cathode is more practical, and the study of $LiFeF_3$ and $NaFeF_3$ should be of great importance in developing the next-generation Li/Na-ion battery with large capacity. We have reported the preparation of $NaFeF_3$ prepared by mechanochemical synthesis with a discharge capacity of 120 mAh g^{-1} at around 2.7 V, which corresponds to 61% of the theoretical capacity (197 mAh g^{-1}) [7]. The reason for this poor efficiency rate is that the mechanochemically

* Corresponding author. Tel.: +81 92 583 7841; fax: +81 92 583 7841.
E-mail address: s-okada@cm.kyushu-u.ac.jp (S. Okada).

0378-7753/$ – see front matter © 2011 Elsevier B.V. All rights reserved.
doi:10.1016/j.jpowsour.2011.09.064

synthesized $NaFeF_3$ had relatively lower crystallinity and Fe^{3+} was partially contained in an amorphous phase. In further investigations, we recently carried out a unique study of highly dispersed uniformly sized perovskite-type $NaFeF_3$ prepared by liquid-phase synthesis using a high-boiling-point organic solution in which uniformly sized $NaFeF_3$ with ca. 10–20 nm showed a large discharge capacity at a high discharge rate [8]. From these previous studies, the crystallographic features of cathode active materials were found to have a significant influence on the electrochemical properties.

In the present study, to determine the electrochemical influence of the crystallinity, we prepared highly crystalline $NaFeF_3$ annealed after roll-quenching and investigated its electrochemical properties and structural changes during charge–discharge measurements by ex situ XRD analysis.

2. Experimental

2.1. Preparation of $NaFeF_3$ using the roll-quench method

$NaFeF_3$ was prepared from a stoichiometric mixture of FeF_2 (SOEKAWA Chemicals Ltd.) and $NaHF_2$ (SOEKAWA Chemicals Ltd.) or NaF (SOEKAWA Chemicals Ltd.) with a molar ratio of FeF_2:NaF/$NaHF_2$ = 1:1. The mixture was ground in an Ar-filled glove box and placed in a Pt tube covered silica tube. The Pt and silica tubes have a small hole of 0.3 mm in diameter at the bottom to inject the melted sample to a single copper roller. In the roll-quench machine (Harddays Co. Ltd.), the powder sample was heated by the joule heat of induction current in Pt tube. After heating over 1000 °C for 40 s, the melted mixture was injected by high pressure Ar gas and quenched onto a single copper roller with rotation at 2000 rpm in Ar atmosphere. Flake like quenched samples were collected in the Ar chamber.

The overall reaction schemes of the obtained $NaFeF_3$ are:

$$FeF_2 + NaHF_2 \rightarrow NaFeF_3 + HF$$

$$FeF_2 + NaF \rightarrow NaFeF_3$$

Hereinafter, the obtained $NaFeF_3$ samples prepared with $NaHF_2$ and NaF are referred to as $NaFeF_3$ (obtained from $NaHF_2$) and $NaFeF_3$ (obtained from NaF), respectively, and $NaFeF_3$ refers to the both samples except as otherwise noted.

The 70 wt.% obtained $NaFeF_3$ powder was dry-ball-milled with 25 wt.% acetylene black (AB, Denki Kagaku Co. Ltd.) in Ar atmosphere. Cathodes were fabricated by mixing the $NaFeF_3$/C composite powder with a 5 wt.% PTFE Teflon binder (Daikin Industry Ltd.) and punched in the form of disks (ca. 30 mg in weight and 10 mm in diameter). They were dried at approximately 120 °C overnight under vacuum before assembling the cells. The electrochemical performance of the $NaFeF_3$ was evaluated with a 2032 coin-type cell using a non-aqueous electrolyte (1 M $NaClO_4$/EC:DMC = 1:1 in volume, Tomiyama Pure Chemicals Co.) and a polypropylene separator (Celgard 3501) against sodium metal (Aldrich). All the cells were assembled in an Ar-filled glove box. The charge–discharge measurement was performed in galvanostatic mode at a rate of 0.076 mA cm^{-2} (0.014 C:1 C rate corresponds to a current rate of 197 mA g^{-1}, which in the ideal case gives complete discharge in 1 h) in the potential window between 1.5 and 4.5 V. The test temperature was 25 °C.

The electrodes were carefully taken out from the cells in the Ar-filled glove box, washed, and immersed with DMC for one night to remove the electrolyte, and dried prior to being set in an Ar-filled transfer vessel for XPS or in an Ar-filled cell for XRD.

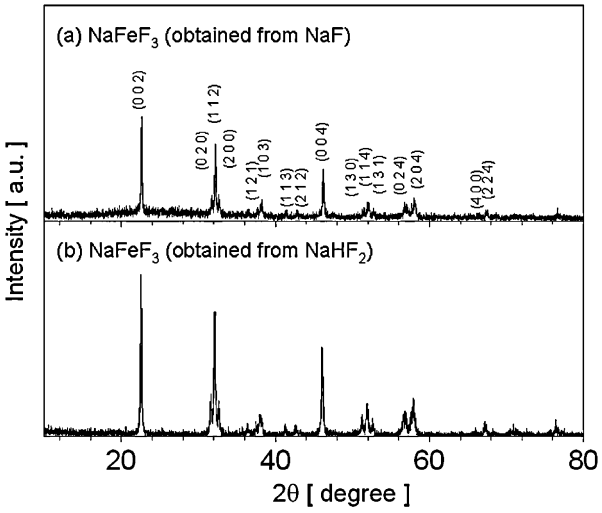

Fig. 1. X-ray diffraction patterns of (a) $NaFeF_3$ (obtained from NaF) and (b) $NaFeF_3$ (obtained from $NaHF_2$).

2.2. Physical characterization

The characterization of the prepared $NaFeF_3$ powder and pellets after charge or discharge processes was carried out with an X-ray powder diffractometer (XRD, 50 kV and 300 mA, Cu Kα, Rigaku TTRIII). The XRD data for the pellet samples was taken under Ar atmosphere because of instability of divalent iron valence in air. The composition of $NaFeF_3$ powder and pellets was determined by means of an atomic absorption spectrometry (AAS, Z-2300, Hitachi) following the pretreatment with the conc. HCl solution. X-ray photoelectron spectroscopy (XPS) was carried out with JPS-9000 (JEOL Ltd.) using focused monochromatized Mg Kα radiation ($h\nu$ = 1253.6 eV).

3. Results and discussion

The crystal structure of the obtained $NaFeF_3$ was characterized with XRD. The XRD patterns for the $NaFeF_3$ (obtained from NaF) and $NaFeF_3$ (obtained from $NaHF_2$) powders are shown in Fig. 1. All the peaks correspond to a single phase and can be indexed as an orthorhombic structure with space group *Pnma*. No other impurity phases such as FeF_2 were detected from the analysis. As shown in Table 1, $NaFeF_3$ obtained from $NaHF_2$ was in agreement from the literature value (ICDD 043-0705). However, as for the $NaFeF_3$ (obtained from NaF) sample, high background with a halo peak at 2θ = 20–40° was observed, and the peaks are broader than that of $NaFeF_3$ (obtained from $NaHF_2$), indicating lower crystallinity and an amorphous component consist in $NaFeF_3$ (obtained from NaF). According to these lattice constants, the each axis of $NaFeF_3$ extends with a decrease of its crystallinity, and thus the unit cell volume increases.

Fig. 2 shows the initial charge (Na extraction) and discharge (Na insertion) curves of the obtained $NaFeF_3$. The charge–discharge cycle tests were performed at a rate of 0.076 mA cm^{-2} between 1.5 V and 4.0 V. The first charge and discharge capacity of $NaFeF_3$ (obtained from NaF) was 130 mAh g^{-1} and 110 mAh g^{-1} with an

Table 1
Lattice constants of $NaFeF_3$ powder samples obtained from NaF and $NaHF_2$.

	a/Å	b/Å	c/Å	α/°	Unit cell volume/Å^3
$NaFeF_3$ (obtained from NaF)	5.51	5.66	7.86	90.0	245.3
$NaFeF_3$ (obtained from $NaHF_2$)	5.50	5.65	7.86	90.0	244.9
$NaFeF_3$ (ICDD 043-0705)	5.48	5.66	7.88	90.0	244.4

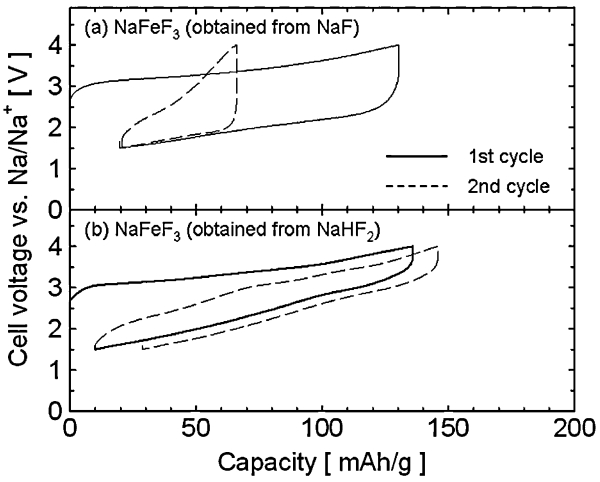

Fig. 2. First and second charge and discharge curves of (a) $NaFeF_3$ (obtained from NaF) and (b) $NaFeF_3$ (obtained from $NaHF_2$) at a rate of 0.076 mA cm^{-2} between 1.5 and 4.0 V vs. Na/Na^+.

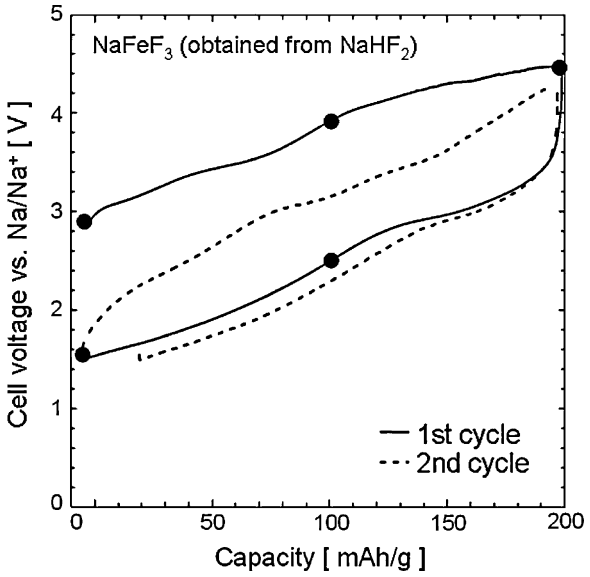

Fig. 3. First and second charge and discharge curves of $NaFeF_3$ (obtained from $NaHF_2$) at a rate of 0.076 mA cm^{-2} between 1.5 and 4.5 V vs. Na/Na^+. The symbols (●) represent the sampling points for the XPS (Fig. 4) and ex situ XRD measurement (Fig. 5).

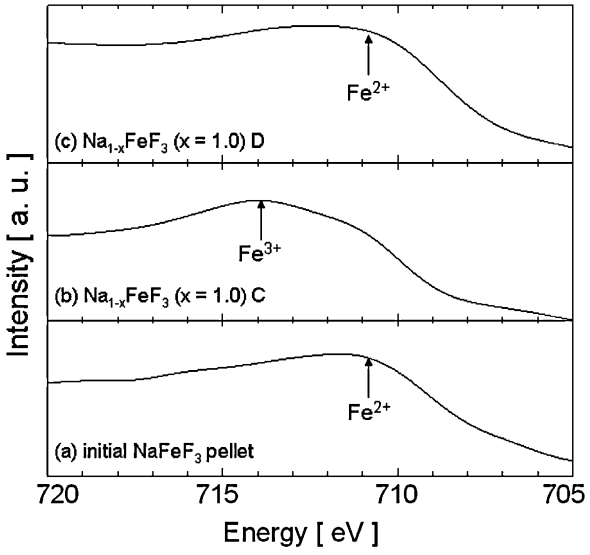

Fig. 4. XPS spectra of $NaFeF_3$ (obtained from $NaHF_2$) during the first charge/discharge cycle (a) initial $NaFeF_3$ pellet, (b) $Na_{1-x}FeF_3$ ($x = 1.0$) C, and (c) $Na_{1-x}FeF_3$ ($x = 0.0$) D, respectively.

84.6% discharge/charge efficiency. In contrast, $NaFeF_3$ (obtained from $NaHF_2$) showed the first charge and discharge capacities of 136 mAh g^{-1} and 126 mAh g^{-1} with a 92.6% discharge/charge efficiency. Given the results for the $NaFeF_3$ samples with different crystallinity and a previous study of $NaFeF_3$ prepared by mechanochemical synthesis [7], the capacity of $NaFeF_3$ has been improved by increasing the crystallinity of $NaFeF_3$. However, the discharge capacities of $NaFeF_3$ (obtained from $NaHF_2$) and $NaFeF_3$ (obtained from NaF) correspond to only 64.0% and 55.8% of the theoretical capacity of $NaFeF_3$, and further improvement could be achieved using different approaches. The charge–discharge voltage range is a key factor in determining battery properties such as capacity and battery life. To increase the rechargeable capacity, the charge cutoff voltage for $NaFeF_3$ was changed up to 4.5 V. In the discharge profile of the first and second cycles (Fig. 3), the cell voltage of $NaFeF_3$ (obtained from $NaHF_2$) gradually decreased to 1.5 V through an inflection point at around 2.7 V, the same as the measurement at a range of 1.5–4.0 V. The $NaFeF_3$ gives rise to an initial charge and discharge capacity of 197 mAh g^{-1} and 197 mAh g^{-1}, respectively, achieving a discharge efficiency of 100%, which is improved from that tested between 1.5 and 4.0 V. In addition, the $NaFeF_3$ tested in this voltage range showed a much better efficiency of 89.4% in the second cycle (second charge and discharge capacity of 197 mAh g^{-1} and 170 mAh g^{-1}). The results of the AAS measurement suggest that this charge–discharge reaction has occurred with extraction/insertion of sodium during cycling, as shown in Table 2.

The Fe 2p XPS peaks of $NaFeF_3$ (obtained from $NaHF_2$) were analyzed to examine the oxidation states after initial charge or discharge. Fig. 4 shows the Fe 2p spectra of (a) initial $NaFeF_3$ pellet, (b) 1 Na initial charged pellet ($Na_{1-x}FeF_3$ ($x = 1.0$) C), and (c) 1 Na discharged pellet after 1 Na initial charge ($Na_{1-x}FeF_3$ ($x = 0.0$) D), respectively. The Fe^{2+} spectrum consists of two peaks due to spin-orbit coupling of Fe $2p_{3/2}$ and $2p_{2/1}$. $2p_{3/2}$ and $2p_{1/2}$ peaks of Fe^{2+} locate at 710.8 and 723.9 eV, respectively. For Fe^{3+}, the $2p_{3/2}$ and $2p_{1/2}$ peaks shift to 713.9 and 727.6 eV. The obtained XPS data of initial, initial charged, and discharged pellets shows that the iron oxidation state was changed from Fe^{2+} to Fe^{3+} during initial charge and returned to the original Fe^{2+} state at the end of first cycle, reversibly. However, as shown in Fig. 3, the second charge profile was not same to the initial charge profile, which suggests that the structure of $NaFeF_3$ was changed somewhat by the first charge/discharge cycle. To confirm the structure change of the cathode on the first cycle, the ex situ XRD measurements for $Na_{1-x}FeF_3$

Table 2
Correlation between the amount of electron transfer and the detected Na content in cathode pellet by AAS measurement during first cycle.

$Na_{1-x}FeF_3$ at various state of charge	Chemical composition estimated by charge/discharge capacity	Detected Na content by AAS measurement [Na]/[FeF_3]
0.5 Na charged state	$Na_{0.5}FeF_3$	0.49
Initial charged state up to 4.5 V	$Na_{0.31}FeF_3$	0.27
Discharged state down to 1.5 V after initial charge	$Na_{0.88}FeF_3$	0.96

Table 3
Lattice constants of $Na_{1-x}FeF_3$ during charge–discharge cycle.

	a/Å	b/Å	c/Å	α/°	Unit cell volume/Å^3
Initial $NaFeF_3$ cathode pellet mixed with AB	5.46	5.66	7.89	90.0	243.8
1 Na initial charged $Na_{1-x}FeF_3$ (x = 1.0)	5.50	5.63	7.78	90.0	240.9
1 Na discharged $Na_{1-x}FeF_3$ (x = 0.0) after initial charge	5.49	5.68	7.90	90.0	246.3

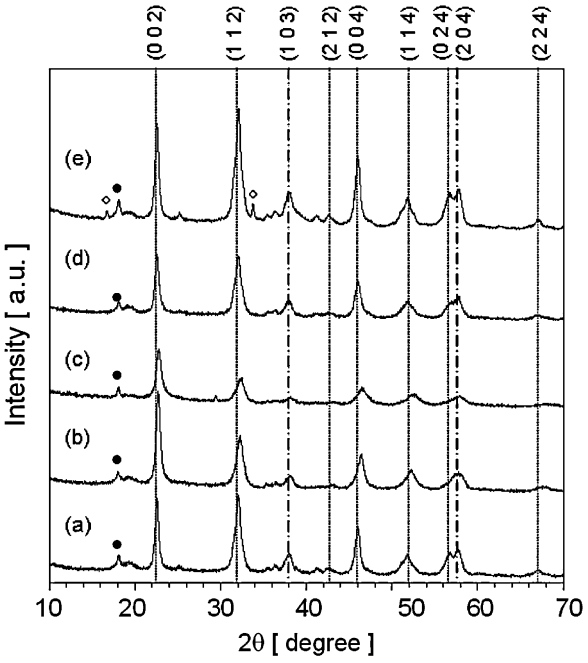

Fig. 5. Ex situ X-ray diffraction patterns of $NaFeF_3$ (obtained from $NaHF_2$) during the first charge/discharge cycle (a) initial $NaFeF_3$ state, (b) $Na_{1-x}FeF_3$ (x = 0.5) C, (c) $Na_{1-x}FeF_3$ (x = 1.0) C, (d) $Na_{1-x}FeF_3$ (x = 0.5) D, and (e) $Na_{1-x}FeF_3$ (x = 0.0) D, respectively. The symbols (◊) represent unknown peaks. While the peaks shown by the dotted line shifted reversibly during cycle, the peaks shown with the chain lines were moving little.

(obtained from $NaHF_2$) pellets were performed at 5 points, initial state ($Na_{1-x}FeF_3$ (x = 0.0) → 0.5 Na initial charged state ($Na_{1-x}FeF_3$ (x = 0.5) C) → 1 Na initial charged state ($Na_{1-x}FeF_3$ (x = 1.0) C) → 0.5 Na discharged state ($Na_{1-x}FeF_3$ (x = 0.5) D) → 1 Na discharged state ($Na_{1-x}FeF_3$ (x = 0.0) D), as shown in Fig. 3 under an Ar atmosphere.

Most of the XRD peaks such as (1 1 2), (0 0 4) and (1 1 4) moved to higher 2θ angle from that of the initial state on initial charge process (Fig. 5 (a) → (b) → (c)). After 1 Na initial charge, the XRD peaks moved back to almost the original position of the initial state during discharge process. In contrast, the XRD peaks of (1 0 3) and (2 0 4) were hardly seen to move on cycle. It means that the lattice behaviors of a axis and c axis are opposite direction. As actually shown in Table 3, while the lattice constants of b axis and c axis were decreasing with charge, a axis increased. These results mean that the corner-sharing matrix of $NaFeF_3$ is stable enough to maintain the charge–discharge cycle by lattice vibration accompanying the extraction/insertion of sodium. In addition, the discrepancy of the unit cell volume between $NaFeF_3$ powder (Table 1) and the cathode pellet (Table 3) suggests the small quantity release of fluorine during mixing process with AB. In Fig. 5, the peak intensity for (1 1 2), (0 0 4) and (0 2 4), which includes sodium at the *4c* site, increased and decreased by associating with charge–discharge processes. To determine the reason for this intensity change, we performed a simulation using the RIETAN-FP program [9]. When an element at the *4c* site was changed to empty from sodium, the intensity of peak for (1 1 2), (0 0 4) and (0 2 4) in the simulated XRD profile was decreased like the behavior of Fig. 5, indicating that sodium at *4c* site of $NaFeF_3$ can extract/insert reversibly. The XRD data of charged/discharged pellets suggests that the extracted sodium turned back to the *4c* site. However, small unknown phases were also detected on the XRD profile at the end of the first cycle ($Na_{1-x}FeF_3$ (x = 0.0) D). According to our previous paper [5], FeF_3 begins a conversion reaction below 2 V against Li anode. Although the average working voltage of Na-ion battery is 0.5 V lower than that of Li-ion battery, the small other peak at discharged state down to 1.5 V may be the trace of the conversion reaction.

4. Conclusion

A novel synthesis method for $NaFeF_3$ has been developed, and its electrochemical properties were investigated. The single phase of $NaFeF_3$ was successively prepared using the roll-quench method. The initial discharge efficiency of $NaFeF_3$ has been improved by increasing the crystallinity of $NaFeF_3$. The obtained $NaFeF_3$ achieved a charge/discharge efficiency of 100% with an initial charge and discharge capacity of 197 mAh g^{-1} at a rate of 0.076 mA cm^{-2} between 1.5 V and 4.5 V. Fe^{2+}/Fe^{3+} reversible redox reaction on cycle was confirmed by XPS. In addition, XRD measurement proved that $NaFeF_3$ can proceed the extraction/insertion of sodium by the reversible lattice vibration due to the structure strength and flexibility of the corner-sharing matrix, and the extracted sodium has returned to the original *4c* site on discharge.

Acknowledgments

This work was financially supported by the Research & Development Initiative for Scientific Innovation of New Generation Batteries (RISING project) of the New Energy and Industrial Technology Development Organization (NEDO).

References

[1] M.S. Whittingham, Prog. Solid State Chem. 12 (1978) 41.
[2] T.B. Kim, J.W. Choi, H.S. Ryu, G.B. Cho, K.W. Kim, J.H. Ahn, K.K. Cho, H.J. Ahn, J. Power Sources 174 (2007) 1275.
[3] F. Badway, N. Pereira, F. Cosandey, G.G. Amatucci, J. Electrochem. Soc. 150 (2003) A1209.
[4] H. Arai, S. Okada, Y. Sakurai, J. Yamaki, J. Power Sources 68 (1997) 716.
[5] M. Nishijima, I.D. Gocheva, S. Okada, T. Doi, J. Yamaki, T. Nishida, J. Power Sources 190 (2009) 558.
[6] M. Bervas, F. Badway, L.C. Klein, G.G. Amatucci, Electrochem. Solid-State Lett. 8 (2005) A179.
[7] I.D. Gocheva, M. Nishijima, T. Doi, S. Okada, J. Yamaki, T. Nishida, J. Power Sources 187 (2009) 247.
[8] Y. Yamada, T. Doi, I. Tanaka, S. Okada, J. Yamaki, J. Power Sources 196 (2011) 4837.
[9] F. Izumi, K. Momma, Solid State Phenom. 130 (2007) 15.